IEEE Robotics and Automation Letters (RA-L) paper, presented at ICRA 2026, Vienna, Austria. Cite as RA-L paper.

Mechanistic Analysis of Cable Tension Effects on the Stiffness of Cable-Driven Serpentine Manipulators

Yicheng Dai, Sheng Wang, Xin Wang, Han Yuan*, *Member, IEEE,*

***Abstract*—This paper presents a mechanistic analysis of stiffness in cable-driven serpentine manipulators (CDSMs), incorporating both cable tension and cable stiffness. First, we derive an analytical stiffness model based on robot statics, identifying cable tension and stiffness as the dominant factors governing robot stiffness at a given configuration. Crucially, we characterize a previously overlooked tension-stiffness coupling effect: cable tension induces nonlinear stiffness variations in driving cables, significantly altering the overall robot stiffness. Due to this interdependence, quantifying cable tension's specific influence on stiffness remains a challenging research gap. To address this, simulations and experiments validate the model and quantify their coupled effects on robotic stiffness. Results demonstrate that for CDSMs using multi-strand cables with nonlinear stiffness, robot stiffness increases sharply with rising tension. Conversely, when cable elasticity is constant, robot stiffness decreases with increasing tension. These findings provide critical insights for advancing stiffness control accuracy in CDSMs.**

***Index Terms*—Cable-driven serpentine manipulators (CDSMs), stiffness analysis, tensile stiffness, cable tension.**

I. Introduction

CABLE-driven serpentine manipulators (CDSMs) offer high effectiveness for minimally invasive surgeries [1], [2] and industrial maintenance [3], [4], as they can operate efficiently in complex and confined environments [5]–[7]. During operation, high stiffness ensures positional accuracy and load capacity, while low stiffness facilitates safety and compliance. Consequently, achieving accurate variable stiffness control is critical for the performance of CDSMs.

Previous literature has shown multiple approaches to CDSM stiffness adjustment. The first prominent strategy involves integrating dedicated variable stiffness devices. These methods, while effective, often share a common limitation: increased structural complexity. This trade-off is evident in several designs. Mechanisms that introduce locking or friction-based actuation, such as the embedded shape memory alloy (SMA) springs by Chengao et al. [8] and the winding-styled rope mechanism by Peiyi et al. [9]. The first one use SMA to actuate a lever mechanism to lock the driving rods. The second one is inspired by snake's behavior and it can increase the friction against the movement of the rod-driven robot. Although these methods can effectively increase stiffness but at the cost of adding significant weight and complexity to the robot's structure.

Designs incorporating spring-based devices, including the torsion spring mechanism by Lim et al. [10] and the nonlinear springs employed by Sobue et al. [11] and other similar devices [12], [13], offer significant stiffness regulation. However, they typically lead to an increased size or the structural complexity in the drive unit. This category also includes flexure-based mechanisms like the one proposed by Jun et al. [14], which, despite providing a linear relationship between deformation and its stiffness for precise variable stiffness control, inevitably adds components and complexity. A distinct method proposed by Nelson [15] utilizes pulley-based force amplification and geometric constraint adjustment. While adjusting cable tension shows potential for regulating robot stiffness, yet the extent and mechanism of its effect warrant further in-depth analysis. In contrast, the geometric constraint adjustment method has demonstrated clear efficacy. However, when applied to CDSMs, additional considerations must be devoted to addressing the structural complexity.

To circumvent the complexity of added mechanisms, alternative research focuses on leveraging the CDSMs' intrinsic properties for stiffness variation. This line of inquiry primarily explores the relationship between robot configuration and cable tension. Although the configuration of a CDSM has been found has strong relationship with the robot stiffness [16], it has limited effect in task scenarios where the shape of the robot cannot be significantly changed. As for the effect of cable tension, Aliakbar et al. [17] proposed using the antagonistic cable tensions to change the robot's stiffness. However, it will increase the energy consumption of the robot. During stiffness analysis of a hyper-redundant CDSM, Mu et al. [18] demonstrated a positive relationship between cable tension and robot stiffness. However, a critical gap persists across this study: they largely model driving cables as idealized springs, overlooking the non-constant, nonlinear stiffness inherent to multi-strand steel cables commonly used in CDSMs. This oversight, as seen

Manuscript received: July 7, 2025; Revised: September 28, 2025; Accepted: November 9, 2025.

This work was supported by the National Natural Science Foundation of China (Grants No. 62573162 and No. 62173114), Guangdong Basic and Applied Basic Research Foundation (Grant No. 2024A1515011228), the Shenzhen Science and Technology Program (Grant No. KJZD20240903100501002, No. JCYJ20250604180218024 and No. GXWD20231129174132001).

Y. Dai, S. Wang, X. Wang and H. Yuan are with the School of Mechanical Engineering and Automation, Harbin Institute of Technology Shenzhen, Shenzhen, PR China. Y. Dai are also with the Tsinghua Shenzhen International Graduate School, Shenzhen, PR China. H. Yuan are also with the Guangdong Provincial Key Laboratory of Intelligent Morphing Mechanisms and Adaptive Robots, and Key University Laboratory of Space Mechanisms and Robots of Guangdong, 518055 Shenzhen, China. (e-mail: daiyicheng94@gmai.com; wangsheng@stu.hit.edu.cn; wangxinsz@hit.edu.cn; yuanhan@hit.edu.cn;). Corresponding author: H. Yuan.

Digital Object Identifier (DOI): see top of this page.

IEEE Robotics and Automation Letters (RA-L) paper, presented at ICRA 2026, Vienna, Austria. Cite as RA-L paper.

in the simulation-based study by Yang et al. [19] which lacked experimental validation, can lead to significant inaccuracies in stiffness analysis. Therefore, a comprehensive investigation that explicitly integrates the coupled effects of both cable tension and the intrinsic nonlinear cable stiffness is imperative for accurate modeling and effective control.

The primary contributions of this paper are as follows:

- An analytical stiffness model for general CDSMs incorporating cable tension and cable stiffness properties.
- Characterization of tensile stiffness variation in multi-strand cables and its integration into CDSM stiffness analysis.
- Quantitative mechanistic analysis of cable tension's influence on CDSM stiffness.

The remainder of this paper is organized as follows: Section 2 details the CDSM kinematic model. Section 3 establishes the static model and derives the stiffness formulation. Section 4 analyzes cable tension and stiffness effects via simulation. Experimental validation is presented in Section 5, with conclusions in Section 6.

II. Kinematic Model

In this paper, a typical CDSM is introduced for kinematic modeling, with its structure depicted in Fig. 1. The corresponding Denavit–Hartenberg (D-H) parameters are shown in Table I.

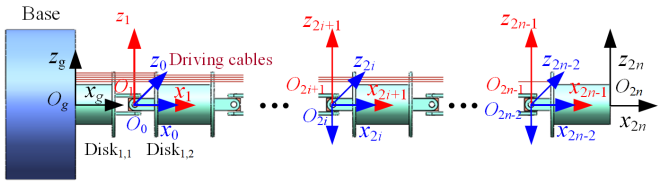

Fig. 1. Schematic of a general cable-driven serpentine manipulator.

TABLE I
D-H parameters of the virtual CDSM.

Joint number	coordinate R_i	α_i	a_i	θ_i	d_i
0	0	-90°	L_0	0	0
1	1	90°	0	$\theta_{1,1}$	0
	2	-90°	L_1	$\theta_{1,2}$	0
2	3	90°	0	$\theta_{2,1}$	0
	4	-90°	L_2	$\theta_{2,2}$	0
	.....				
n	2n-1	90°	0	$\theta_{n,1}$	0
	2n	0	L_n	$\theta_{n,2}$	0

According to Fig. 1, each two arms are connected by a joint. Assuming there are n joints and m driving cables per joint, the total number of cables in the robot is $n \times m$. According to the D-H parameters of the CDSM shown in Table I, from arbitrary local coordinate R_i to R_{i-1} $(0 < i < 2n)$, the relevant transformation matrix can be expressed as:

$$ {}^{R_{i-1}}\boldsymbol{T}_{R_i} = \begin{bmatrix} \cos\theta_i & -\cos\alpha_i \sin\theta_i & \sin\alpha_i \sin\theta_i & a_i \cos\theta_i \\ \sin\theta_i & \cos\alpha_i \cos\theta_i & -\sin\alpha_i \cos\theta_i & a_i \sin\theta_i \\ 0 & \sin\alpha_i & \cos\alpha_i & 0 \\ 0 & 0 & 0 & 1 \end{bmatrix} \tag{1} $$

The transformation matrix from R_0 coordinate to the base coordinate R_g can be expressed as:

$$ {}^{R_0}\boldsymbol{T}_{R_g} = \begin{bmatrix} 1 & 0 & 0 & L_0 \\ 0 & 0 & 1 & 0 \\ 0 & -1 & 0 & 0 \\ 0 & 0 & 0 & 1 \end{bmatrix} \tag{2} $$

Then, the transformation matrix from the end local coordinate R_{2n} to the base coordinate R_g can be expressed as:

$$ {}^{R_g}\boldsymbol{T}_{R_{2n}} = {}^{R_g}\boldsymbol{T}_{R_0} \prod_{i=2n}^{0} {}^{R_{i-1}}\boldsymbol{T}_{R_i} \tag{3} $$

Denote the end pose of the robot in R_{2n} coordinate as $\boldsymbol{X}_e$. Then its expression in the base coordinate can be written as:

$$ \boldsymbol{X} = {}^{R_g}\mathbf{T}_{R_{2n}} \boldsymbol{X}_{\boldsymbol{e}} \tag{4} $$

Assuming the vector of cable length is $\boldsymbol{L}$ and the vector of joint angle is $\boldsymbol{\theta}$. The mapping from the driving cable space to the joint space can be expressed as:

$$ \boldsymbol{\theta} = f_{\boldsymbol{l},\boldsymbol{\theta}}(\boldsymbol{L}) \tag{5} $$

Since the number of cables exceeds the number of degrees of freedom (DOF) of the robot, the approximate solution of eq. (5) is determined using optimization algorithms, such as the nonlinear least-squares algorithm. Once the joint angles are obtained, the forward kinematics of the CDSM, which maps the joint space to the task space, can be expressed as:

$$ \boldsymbol{X} = f_{\text{fwd}}(\boldsymbol{\theta}) \tag{6} $$

If the manipulator is not redundant driven, $m = n$. Then eq. (5) has a unique solution. If the robot is redundant driven, $m > n$. Equation (5) has multiple solutions and optimized solution can be found based on minimum norm method. On the contrary, the inverse kinematic is the inverse process of eq. (5) and it can be expressed as:

$$ \boldsymbol{\theta} = f_{\text{inv}}(\boldsymbol{X}) \tag{7} $$

Usually, optimization functions such as the minimum norm method will be used to obtain the desired set of solutions based on specific objectives and constraints. After knowing joint angles, the length of the driving cables can be obtained:

$$ \boldsymbol{L} = f_{\boldsymbol{\theta},\boldsymbol{l}}(\boldsymbol{\theta}) \tag{8} $$

Hence, the kinematic model of the CDSM can be expressed by Eq. (5-8).

III. Statics and Stiffness Modeling

A. Static model

Under the effect of cable tension $\boldsymbol{F_L}$, external wrench $\boldsymbol{W_e}$, and the effect of gravitional Wrench $\boldsymbol{G_g}$, a CDSM can reach static equilibrium. The force status is shown in Fig. 2.

Denote the elongation of driving cables caused by tension as $\delta\boldsymbol{L}$, the pose change of the distal end caused by external wrench as $\delta\boldsymbol{X}$, and the center height change of the links as $\delta\boldsymbol{H}$. According to the virtual work principle:

$$ \boldsymbol{W_e}^{\mathrm{T}} \delta\boldsymbol{X} - \boldsymbol{F_L}^{\mathrm{T}} \delta\boldsymbol{L} - \boldsymbol{G_g}^{T} \delta\boldsymbol{H} = 0 \tag{9} $$

IEEE Robotics and Automation Letters (RA-L) paper, presented at ICRA 2026, Vienna, Austria. Cite as RA-L paper.

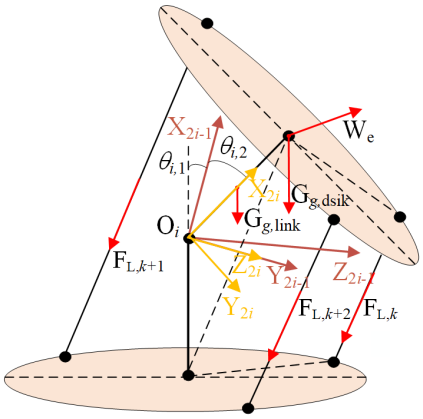

Fig. 2. The force status of the cable driven serpentine manipulator.

Taking the derivative of Eq. (9) with respect to the joint angle $\boldsymbol{\theta}$ and we get:

$$\boldsymbol{W_e}^{\mathrm{T}}\frac{\delta \boldsymbol{X}}{\delta \boldsymbol{\theta}}-\boldsymbol{F_L}^{\mathrm{T}}\frac{\delta \boldsymbol{L}}{\delta \boldsymbol{\theta}}-\boldsymbol{G_g}^{\mathrm{T}}\frac{\delta \boldsymbol{H}}{\delta \boldsymbol{\theta}}=0 \tag{10}$$

Substituting $\frac{\delta \boldsymbol{X}}{\delta \boldsymbol{\theta}} \approx \frac{\partial \boldsymbol{X}}{\partial \boldsymbol{\theta}}$, $\frac{\delta \boldsymbol{L}}{\delta \boldsymbol{\theta}} \approx \frac{\partial \boldsymbol{L}}{\partial \boldsymbol{\theta}}$ and $\frac{\delta \boldsymbol{H}}{\delta \boldsymbol{\theta}} \approx \frac{\partial \boldsymbol{H}}{\partial \boldsymbol{\theta}}$ into Eq. (10), we have:

$$\boldsymbol{W_e}^{\mathrm{T}}\frac{\partial \boldsymbol{X}}{\partial \boldsymbol{\theta}}-\boldsymbol{F_L}^{\mathrm{T}}\frac{\partial \boldsymbol{L}}{\partial \boldsymbol{\theta}}-\boldsymbol{G_g}^{T}\frac{\partial \boldsymbol{H}}{\partial \boldsymbol{\theta}}=0 \tag{11}$$

$$\boldsymbol{W_e}^{\mathrm{T}}\boldsymbol{J_X}-\boldsymbol{F_{\mathrm{L}}}^{\boldsymbol{T}}\boldsymbol{J_L}-\boldsymbol{G_{\mathrm{g}}}^{T}\boldsymbol{J_H}=0 \tag{12}$$

where $\boldsymbol{J_X}=\frac{\partial \boldsymbol{X}}{\partial \boldsymbol{\theta}}$, $\boldsymbol{J_L}=\frac{\partial \boldsymbol{L}}{\partial \boldsymbol{\theta}}$ and $\boldsymbol{J_H}=\frac{\partial \boldsymbol{H}}{\partial \boldsymbol{\theta}}$. They are the Jacobian matrices. Through a mathematical transpose of Eq. (12), we have:

$$\boldsymbol{J_X}^{\mathrm{T}}\boldsymbol{W_e}-\boldsymbol{J_L}^{\mathrm{T}}\boldsymbol{F_L}-\boldsymbol{J_H}^{\mathrm{T}}\boldsymbol{G_g}=0 \tag{13}$$

Equation (13) is the static model, and the cable tension will be obtained while the joint angle and the external force are known.

B. Stiffness model

Based on the static model we can get the stiffness model. Differentiating Eq. (13) and we have:

$$\frac{\partial \boldsymbol{J_X}^{\mathrm{T}}}{\partial \boldsymbol{\theta}}\boldsymbol{W_e}+\boldsymbol{J_X}^{\mathrm{T}}\frac{\partial \boldsymbol{W_e}}{\partial \boldsymbol{\theta}}-\frac{\partial \boldsymbol{J_L}^{\mathrm{T}}}{\partial \boldsymbol{\theta}}\boldsymbol{F_L}-\boldsymbol{J_L}^{\mathrm{T}}\frac{\partial \boldsymbol{F_L}}{\partial \boldsymbol{\theta}}-\frac{\partial \boldsymbol{J_H}^{\mathrm{T}}}{\partial \boldsymbol{\theta}}\boldsymbol{G_g}-\boldsymbol{J_H}^{\mathrm{T}}\frac{\partial \boldsymbol{G_g}}{\partial \boldsymbol{\theta}}=0 \tag{14}$$

$$\boldsymbol{J_X}^{\mathrm{T}}\partial \boldsymbol{W_e}=(\frac{\partial \boldsymbol{J_L}^{\mathrm{T}}}{\partial \boldsymbol{\theta}}\boldsymbol{F_L}+\boldsymbol{J_L}^{\mathrm{T}}\frac{\partial \boldsymbol{F_L}}{\partial \boldsymbol{\theta}}+\frac{\partial \boldsymbol{J_H}^{\mathrm{T}}}{\partial \boldsymbol{\theta}}\boldsymbol{G_g}+\boldsymbol{J_X}^{\mathrm{T}}\frac{\partial \boldsymbol{G_g}}{\partial \boldsymbol{\theta}}-\frac{\partial \boldsymbol{J_X}^{\mathrm{T}}}{\partial \boldsymbol{\theta}}\boldsymbol{W_e})\partial \boldsymbol{\theta} \tag{15}$$

Substituting $\boldsymbol{H_L}=\frac{\partial \boldsymbol{J_L}^{\mathrm{T}}}{\partial \boldsymbol{\theta}}$, $\frac{\partial \boldsymbol{F_L}}{\partial \boldsymbol{\theta}}=\frac{\partial \boldsymbol{F_L}}{\partial \boldsymbol{L}}\frac{\partial \boldsymbol{L}}{\partial \boldsymbol{\theta}}=\boldsymbol{K_L}\boldsymbol{J_L}$, $\boldsymbol{H_H}=\frac{\partial \boldsymbol{J_H}^{\mathrm{T}}}{\partial \boldsymbol{\theta}}$, $\frac{\partial \boldsymbol{G_g}}{\partial \boldsymbol{\theta}}=0$ and $\boldsymbol{H_X}=\frac{\partial \boldsymbol{J_X}^{\mathrm{T}}}{\partial \boldsymbol{\theta}}$ into eq. (15) we have:

$$\boldsymbol{J_X}^{\mathrm{T}}\partial \boldsymbol{W_e}=(\boldsymbol{H_L}\boldsymbol{F_L}+\boldsymbol{J_L}^{\mathrm{T}}\boldsymbol{K_L}\boldsymbol{J_L}+\boldsymbol{H_H}\boldsymbol{G_g}-\boldsymbol{H_X}\boldsymbol{W_e})\partial \boldsymbol{\theta} \tag{16}$$

where $\boldsymbol{H_X}$, $\boldsymbol{H_L}$ and $\boldsymbol{H_H}$ are the Hessian matrices, which represent the differentiation of each Jacobian matrix. $\boldsymbol{K_L}$ is the cable stiffness matrix. Substituting $\partial \boldsymbol{\theta}=\boldsymbol{J_X}^{-1}\partial \boldsymbol{X}$ and $\boldsymbol{K_R}=\frac{\partial \boldsymbol{W_e}}{\partial \boldsymbol{X}}$ into Eq. (16) we have:

$$\begin{aligned}\boldsymbol{K_R}=&(\boldsymbol{J_X}^{\mathrm{T}})^{-1}(\boldsymbol{H_L}\boldsymbol{F_L})(\boldsymbol{J_X})^{-1}+(\boldsymbol{J_X}^{\mathrm{T}})^{-1}(\boldsymbol{J_L}^{\mathrm{T}}\boldsymbol{K_L}\boldsymbol{J_L})(\boldsymbol{J_X})^{-1}\\&+(\boldsymbol{J_X}^{\mathrm{T}})^{-1}(\boldsymbol{H_H}\boldsymbol{G_g}-\boldsymbol{H_X}\boldsymbol{W_e})(\boldsymbol{J_X})^{-1}\end{aligned}$$

where $\boldsymbol{K_R}$ is the robot stiffness matrix in Cartesian space. It should be noted that $(\boldsymbol{J_X}^{\mathrm{T}})^{-1}(\boldsymbol{H_L}\boldsymbol{F_L})(\boldsymbol{J_X})^{-1}$ is noted as active stiffness, and $(\boldsymbol{J_X}^{\mathrm{T}})^{-1}(\boldsymbol{J_L}^{\mathrm{T}}\boldsymbol{K_L}\boldsymbol{J_L})(\boldsymbol{J_X})^{-1}$ is noted as passive stiffness. They are respectively related to cable tension and cable stiffness.

In CDSMs, actuation redundancy yields multiple feasible cable tension sets satisfying static equilibrium. This under determination enables stiffness optimization and control through deliberate tension adjustment. Consequently, a rigorous investigation into cable tension's influence on robotic stiffness is imperative.

IV. Simulation Analysis

Based on the stiffness model established in Section III, the Jacobian and Hessian matrices are fully determined for a given robot configuration. Under such conditions, robot stiffness depends exclusively on cable tension and cable stiffness. This section examines how these parameters affect overall stiffness through numerical simulation. Simulations employ a virtual prototype with 5 joints, where cable routing holes (radius R=30mm) are uniformly distributed on disks separated by 20mm linkages.

A. Effect of cable stiffness on the robot stiffness

The stiffness of the cable is primarily determined by the Young's modulus of the driving cables. In this section, we examine the impact of the cable's Young's modulus on both the passive stiffness component and the overall stiffness of the robot. For the simulation conducted, all the joint angles are set to 10°, with identical cable tensions applied in each case.

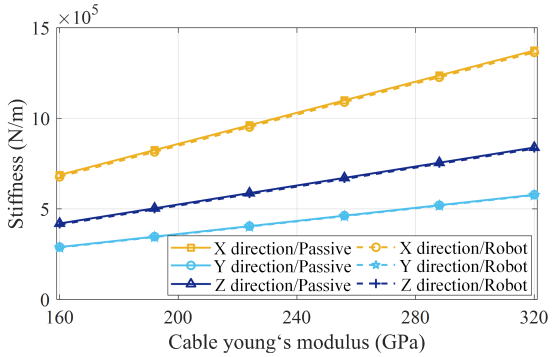

Fig. 3. Effect of cable stiffness on the passive stiffness item and robot stiffness (The cable young's modulus varies from 160GPa to 320Gpa, while cable tension and robot configuration keeps constant. The maximum difference between the passive stiffness value and the robot stiffness value is 1.5%).

As depicted in Fig. 3, simulations demonstrate that robot stiffness increases proportionally with cable stiffness across all directions. Crucially, robot stiffness values show close agreement with passive stiffness values, exhibiting similar growth rates. These results confirm that cable stiffness constitutes a dominant component of overall robotic stiffness, consequently exerting significant influence on the stiffness behavior of CDSMs.

B. Effect of cable tension on the robot stiffness

In this part, the influence of cable tension on the robot stiffness is studied. The configuration of the robot is the same

IEEE Robotics and Automation Letters (RA-L) paper, presented at ICRA 2026, Vienna, Austria. Cite as RA-L paper.

with previous subsection. The cable's young's modulus is set to be 200 Gpa. Based on the static model, the cable tension can be written as:

$$\boldsymbol{F_L} = (\boldsymbol{J_L^{\mathrm{T}}})^{-1}(\boldsymbol{J_X^{\mathrm{T}}}\boldsymbol{W_e} - \boldsymbol{J_H^{\mathrm{T}}}\boldsymbol{G_g}) \tag{17}$$

For a redundantly driven system, there are multiple force sets that satisfy the static equation.Conventionally, tensions are resolved through energy-minimization objectives, typically minimizing the sum of squared cable tensions. By progressively increasing the tension lower bound, we systematically elevate cable tensions while concurrently quantifying both active stiffness components and overall robot stiffness.

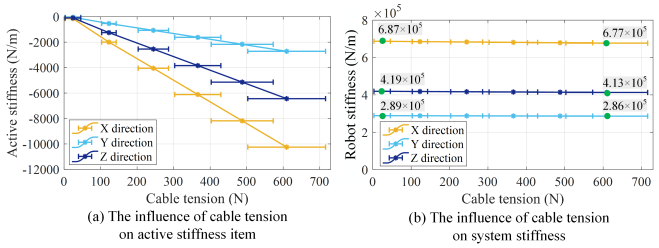

(a) The influence of cable tension on active stiffness item

(b) The influence of cable tension on system stiffness

Fig. 4. The influence of cable tension on the active stiffness item and robot stiffness in different directions (The cable tension varies while cable young's modulus and robot configuration keeps constant. The robot stiffness for x, y and z directions are reduced by 1.46%, 1.04% and 1.43% respectively. The bar of the X-axis represents the scope of cable tension values, which are the result of the calculation of the static equation.).

As illustrated in Fig. 4, an increase in cable tension is associated with a decrease in active stiffness. While cable stiffness keeps constant, the overall robot stiffness shows a modest declining trend. Comparative analysis of Fig. 3 and Fig. 4 reveals that the value of the active stiffness item is small compared to the passive stiffness item and robot stiffness. This observation suggests that active stiffness constitutes a minor proportion of the robot's overall stiffness, indicating a limited impact on the robot stiffness.

Worth noting, the above simulation is carried out with constant cable stiffness. However, real-world CDSMs utilize driving cables exhibiting inherently nonlinear elastic properties—not idealized constant stiffness. Consequently, prior conclusions attributing stiffness increases solely to elevated cable tension may conflate tension effects with variable cable stiffness. This necessitates further mechanistic analysis to isolate cable tension's specific influence on CDSM stiffness.

C. The tensile stiffness of a multi-strand steel cable

To accurately evaluate the influence of cable tension on the stiffness of a CDSM, understanding the mechanical behavior of multi-strand steel cables is crucial. In this study, a tensile test was conducted on a 1×19-strand steel cable with a diameter of 1.2 mm. Based on the obtained force-displacement curve shown in Fig. 5(a), the variation of the cable tensile stiffness can be obtained according to Eq. 18.

$$K_{\mathrm{ts}} = EA = \frac{Fl_0}{\Delta l} \tag{18}$$

where E, A, l_0 and Δl represent the Young's modulus, cross-sectional area, original length and stretch length of the driving cable, respectively.

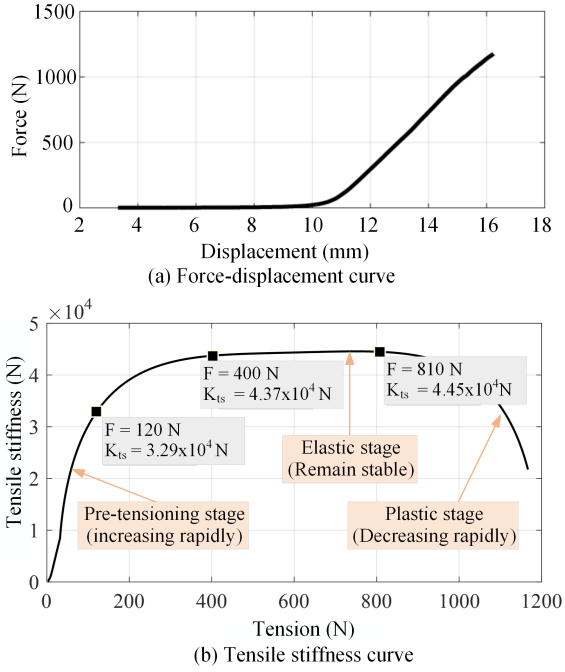

(a) Force-displacement curve

(b) Tensile stiffness curve

Fig. 5. The tensile test result of the 1×19-strand steel cable ((a)The force-displacement curve is obtained directly through the tensile test. (b)According to the definition, the tensile stiffness can be obtained through the slope of each point of the force-displacement curve and the original length of the test cable. In the pre-tensioning stage, cable tensile stiffness increases rapidly.In the elastic stage, cable tensile stiffness remains stable. In the plastic stage, cable tensile stiffness decreases rapidly.).

Then, the mapping between cable tension and tensile stiffness can be obtained through polynomial fitting. To improve fitting accuracy, the tensile stiffness curve is fitted with two polynomials, as shown in Eq. 19. It is worth noting that the mapping of the tension-tensile stiffness for any multi-strand wire cable can be obtained by using this method.

$$K_{ts} = \begin{cases} -1\times10^{-3}F_L^6 + 1.12\times10^{-2}F_L^5 - 0.46F_L^4 + 8.74F_L^3 \\ -70.49F_L^2 + 377.99F_L - 556.89 \qquad (F_L \le 31N) \\ \\ -1.22\times10^{-12}F_L^6 + 4.58\times10^{-9}F_L^5 - 6.94\times10^{-6}F_L^4 \\ +0.0054F_L^3 - 2.26F_L^2 + 493.35F_L - 1924.5 \quad (F_L > 31N) \end{cases} \tag{19}$$

As depicted in Fig. 5(b), the cable tensile stiffness is negligible at small cable tensions. During the pre-tensioning stage, as cable tension increases to 120 N, the tensile stiffness increases exponentially. However, within the tension range of 120 N to 400 N, the increase in tensile stiffness is relative slow. Beyond 400 N and up to 810 N, the cable tensile stiffness stabilizes to a near-constant value. Finally, upon entering the plastic deformation regime, the stiffness undergoes rapid degradation due to material yielding.

D. Effect of cable tension in different cable tensile stages

1) Effect of cable tension in pre-tensioning stage of the cable: Utilizing the obtained tensile stiffness data as the

IEEE Robotics and Automation Letters (RA-L) paper, presented at ICRA 2026, Vienna, Austria. Cite as RA-L paper.

parameter of the driving cables in the CDSM, the robot stiffness can be calculated. Simulation results in Fig. 6 indicate that with an increase in cable tension, the robot stiffness increases by 4.24 times in the x direction, 2.9 times in the y direction, and 4.57 times in the z direction. These results demonstrate that during the pre-tensioning stage of the cable, there is a significant increase in robot stiffness caused by the increased cable tension.

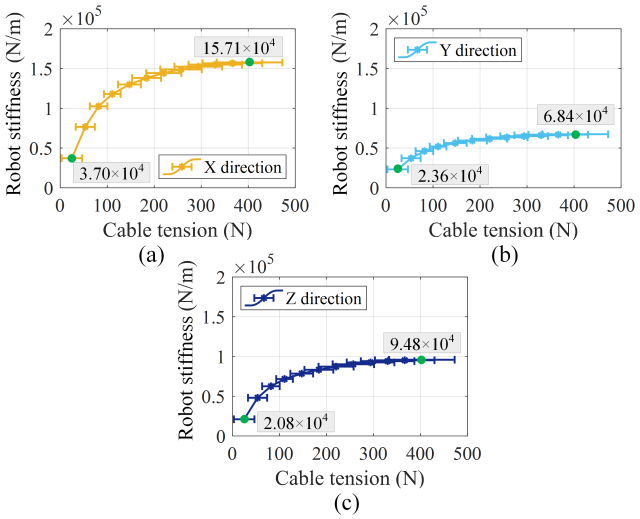

Fig. 6. Stiffness variation of the CDSM as cable tension increases during the pre-tensioning stage of cable (In this simulation case, cable tensile stiffness varies significantly with cable tension. (a,b,c) The robot stiffness increases by 4.24, 2,9 and 4.57 times in the x, y and z directions respectively).

2) Effect of cable tension in elastic stage of the cable: Further simulation is conducted in the elastic stage of the cable. As illustrated in Fig. 7, the robot stiffness exhibits a slight decreasing trend as cable tension increases. Specifically, in the x direction, the robot's stiffness decreases to 98.5%, while in the y and z directions, it reduces to 99.4% and 98.4%, respectively. Compared to the previous simulation results, these findings indicate that when the tensile stiffness of the driving cables remains relatively constant, corresponding to the elastic stage of the cable, an increase in cable tension results in a small decrease in robot stiffness.

3) Effect of cable tension under different robot configurations: In this part, further simulation under different robot configurations is conducted to verify the robustness of the findings under different scenarios. Simulation results are shown in Fig. 8. The robot stiffness in different directions shows the same variation tend: with cable tension increasing, the robot stiffness increases rapidly at first, and then it decreases slightly. By comparing Fig. 5(b) and Fig. 8(d, e, f), it can be found that the robot stiffness and the cable tensile stiffness have similar varying trends. This explains why, in previous studies, higher cable forces were used to enhance the stiffness of the robot—specifically, the increase in tension first leads to an increase in the tensile stiffness of the cable, thereby raising the overall stiffness of the robot. However, since prior research overlooked the variability of the cable's tensile stiffness, it could only conclude that increasing cable tension enhances the stiffness of the manipulator system. Although this

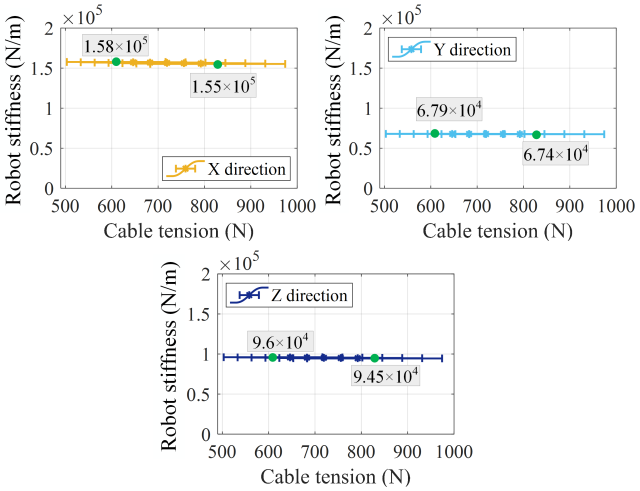

Fig. 7. Stiffness variation of the CDSM as cable tension increases during the elastic stage of cable (In this simulation case, the cable is at its elastic stage and its tensile stiffness remains constant. (a,b,c) The robot stiffness is reduced by 1.5%, 0.6% and 1.6% in the x, y and z directions respectively.).

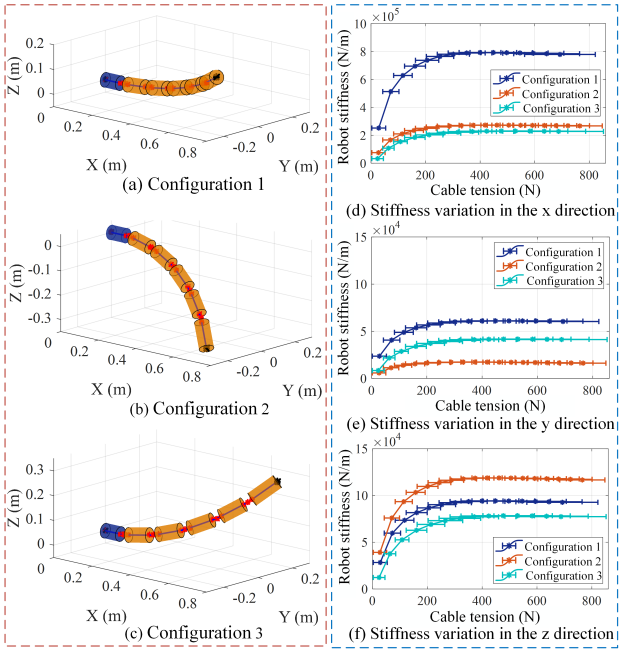

Fig. 8. Stiffness variation of the CDSM as cable tension increases under different configurations ((a,b,c) Different robot configurations. (d,e,f)The robot stiffness variation in the x, y and z directions. With cable tension increasing, at first the robot stiffness increases rapidly. Then it decreases slightly.).

conclusion is correct, the underlying adjustment mechanism was not clearly explained, and its applicability is limited to the pre-tensioning stage of the cable, rather than all working conditions. For example, when the cable is in the elastic stage—i.e., when its tensile stiffness remains relatively constant—an increase in cable tension has a minor effect on the manipulator's stiffness and may even cause a slight reduction, as shown in the latter segments of the curves in Fig. 8(d, e, f). The above analysis provides important insights for achieving wide-range stiffness control of CDSMs, ensuring their stable operation in confined environments.

IEEE Robotics and Automation Letters (RA-L) paper, presented at ICRA 2026, Vienna, Austria. Cite as RA-L paper.

V. Experimental Verification

A. Experimental setup

For validation, a CDSM prototype has been constructed, as shown in Fig. 9. To minimize frictional effects and accurately assess the impact of cable tension on robot stiffness, a friction-reducing device is installed at each cable hole, as illustrated in the upper right corner of Fig. 9. Each joint has a single degree of freedom, and the rotational angle range is limited to ±30°. The joint is driven by two symmetrically distributed cables where one cable is position controlled and the other one is force controlled. To mitigate interference between the driving cables, adjacent joints are arranged with a 30° twist along the length of the robot, as shown in Fig. 9.

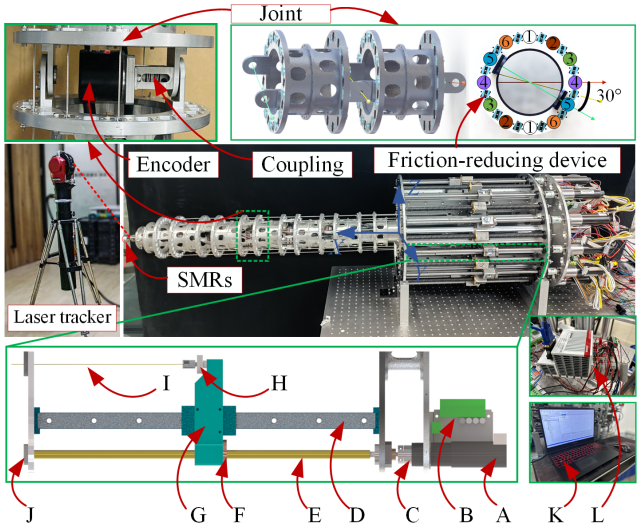

Fig. 9. The prototype of the CDSM.

B. Experimental validation of the analytical stiffness model

The first is the validation of the established stiffness model. To further minimize the effect of friction between the cables and the multiple cable holes, the verification will be carried out on a robotic arm consisting of three joints. Standard weights were vertically suspended from the end of the CDSM and its position change was measured by the laser tracker. Then the compliance of the CDSM can be obtained according to Eq.20. Set the same joint angles and cable tension in the simulation model and the the robot compliance and stiffness can be calculated.

$$C = \frac{\Delta X_e}{\Delta F}, K = C^{-1} \tag{20}$$

where ΔF is external load and ΔX_e is the resulted displacement. C and K represent the compliance and stiffness of CDSM, respectively.

In this section, the stiffness in the z direction is used to evaluate the model accuracy. The measured stiffness is 0.131 N/mm and the calculated value is 0.139 N/mm. Therefore, the error between the model and the ground truth is 5.75%, indicating the high accuracy of the established stiffness model.

C. Verification on the effect of cable tension in pre-tensioning stage

To demonstrate the influence of cable tension on CDSMs when cable stiffness is variable, the previously tested multi-strand steel wire will be used as driving cable.

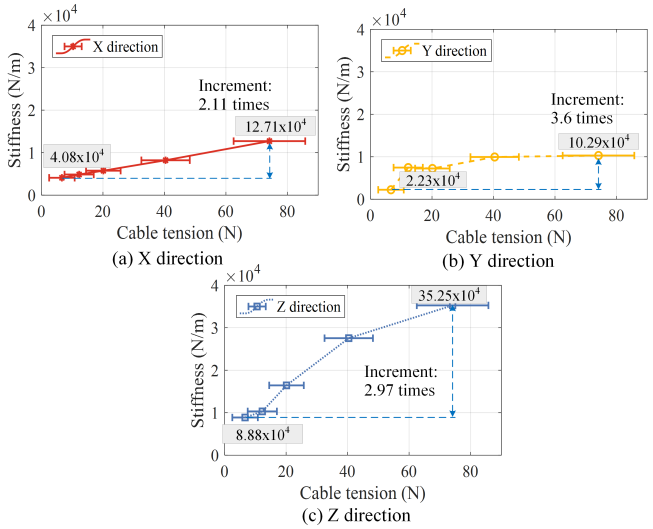

Fig. 10. Effect of cable tension on the robot stiffness during the pre-tensioning stage of cable (The robot stiffness in the x, y and z directions is increased by 2.11, 3.6, and 2.97 times respectively. The stiffness values in the y direction are smaller than the other two directions, but its stiffness changing rate is the largest.).

The robot is arbitrarily configured at angles of -12°, -18°, and -20°. Then, the stiffness of the robot will be measured and results are shown in Fig. 10. Based on the experimental data, when the cable tension increases from 3N to 86N, the increment of the robot stiffness is 2.11 times in the x direction, 3.6 times in the y direction and 2.97 times in the z direction. These results demonstrate that during the pre-tensioning stage, where cable tension governs nonlinear cable stiffness enhancement, the overall robotic stiffness increases rapidly with tension increasing. Notably, it can be found that the stiffness changing rates are most pronounced in the y direction. Moreover, its stiffness value is relative small which is conductive to the measurement of corresponding displacement. This directional anisotropy indicates that the y direction is the optimal axis for observing tension-stiffness coupling effects. Consequently, subsequent analysis focuses primarily on the stiffness in the y direction.

Experimental results confirm that during the pre-tensioning stage, cable tension exerts a profound influence on the stiffness of CDSMs employing multi-strand cables. Specifically, robot stiffness increases nonlinearly with rising tension—consistent with prior observations. Crucially, we attribute this phenomenon primarily to the tension-induced augmentation of cable tensile stiffness, which amplifies dramatically in the pre-tensioning stage. This finding resolves a critical limitation in existing studies, where conventional analyses assume constant

IEEE Robotics and Automation Letters (RA-L) paper, presented at ICRA 2026, Vienna, Austria. Cite as RA-L paper.

cable stiffness. Our work demonstrates that their conclusions hold exclusively within the pre-tensioning stage of the multi-strand cables.

TABLE II
STIFFNESS CHANGE OF THE CDSM IN THE PRE-TENSIONING STAGE OF CABLE (UNIT: N/MM).

	x direction	y direction	z direction
Stiffness	4.08	2.23	8.88
	4.86	7.45	10.31
	5.76	7.24	16.43
	8.21	9.94	27.54
	12.71	10.29	35.25
Increment	2.11 times	3.6 times	2.97 times

D. Verification on the effect of cable tension in elastic stage

In this subsection, the influence of cable tension will be examined when the driving cable maintains stable stiffness. To realize this, hybrid cables are designed by combining steel cables with springs. The measured stiffness of the hybrid cables is presented in Fig. 11.

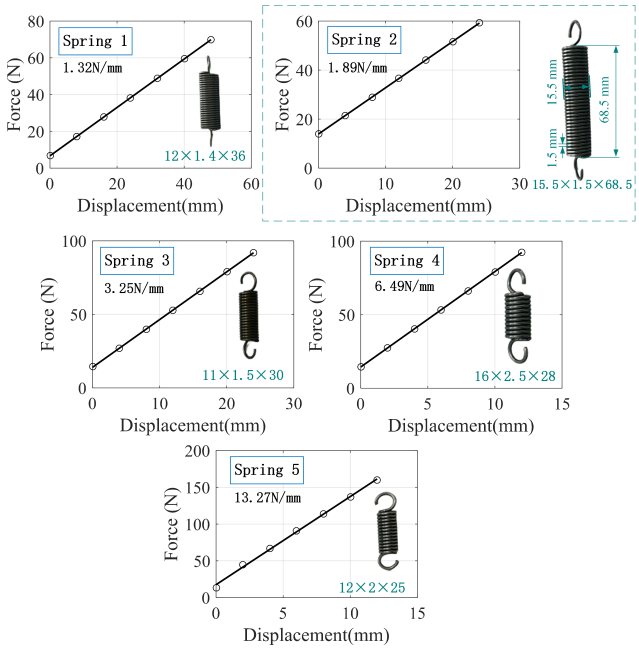

Fig. 11. Stiffness measurement of hybrid cables using different springs (The hybrid cables are made by connecting the steel cables with 5 types of springs respectively.).

In this part, tests will be conducted on robots utilizing hybrid cables with stiffness of 1.89N/mm. The stiffness of the robot will be measured. As evidenced by Fig. 12, the CDSM stiffness in the y direction decreases with increasing cable tension. The maximum observed stiffness reduction rates reach 17% and 40% for the two tested configurations. Contrasted with the results from the pre-tensioning phase, these data demonstrate a significantly diminished influence of cable tension on robot stiffness within the elastic stage. Crucially, we identify a persistent negative correlation between cable tension and robot stiffness in this phase. Consequently, for CDSMs employing cables with constant stiffness, a continuous increase in cable tension could lead to a decrease in robot stiffness.

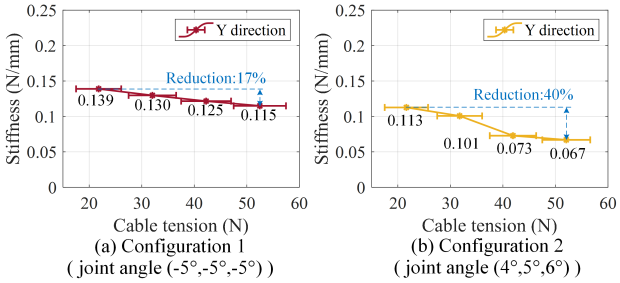

Fig. 12. Effect of cable tension on the robot stiffness during the elastic stage of cable (In this experiment, cable tension varies while cable stiffness remains constant. The maximum stiffness reduction rates are 17% and 40% for the two tested configurations).

E. Verification on the effect of cable stiffness

In this part, the influence of cable stiffness will be investigated. As shown in Fig. 11, five types of hybrid cables with different springs will be used. Then, tests will be conducted with identical cable forces for each configuration.

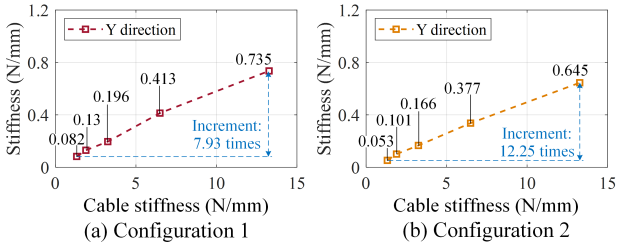

Fig. 13. Effect of cable stiffness on the stiffness of CDSMs (In this experiment, the stiffness of the driving cables is different while cable tensions of each case remains constant. The maximum stiffness increments are 7.93 times and 12.25 times for the two configurations.).

As demonstrated by the experimental results in Fig. 13, the robot's stiffness increases with the stiffness of the hybrid cables. Moreover, the average changing rate in robot stiffness closely approximates that of the hybrid cables. Compared to the influence of cable tension, cable stiffness exerts a more significant effect on the overall robot stiffness.

VI. DISCUSSION

In the above simulation analysis and experimental validation, it is observed that for CDSMs, variations in cable stiffness significantly impact the overall stiffness of the robot. Therefore, analyzing the stiffness characteristics of the cables is crucial for variable stiffness control of CDSMs. In most existing cable-driven robots, multi-strand steel cables—which exhibit nonlinear stiffness behavior—are widely used. For current research on cable-driven robots, this paper highlights a critical limitation: beyond a certain point, further increasing tension becomes ineffective for stiffness enhancement, and it will also leads to excessive energy consumption and heightened risks of cable failure or equipment damage. Moreover,

IEEE Robotics and Automation Letters (RA-L) paper, presented at ICRA 2026, Vienna, Austria. Cite as RA-L paper.

these findings also bear significant implications for the future research. For manipulators requiring high-precision stiffness control, it will be essential to first characterize the cable's stiffness and integrate the coupling effect between tension and stiffness into the control framework. Furthermore, for highly flexible CDSMs that utilize cables with stable elasticity (or operating within their constant-stiffness stage), this paper provide a critical insight: an increase in cable tension may lead to a slight decrease in overall robot stiffness. These results are vital for the control of next-generation manipulators with stringent stiffness control accuracy requirements.

VII. Conclusion

This paper presents a mechanistic analysis of cable tension's effect on the stiffness of CDSMs, explicitly addressing the tension-stiffness coupling effect in driving cables. We develop an analytical stiffness model and employ simulations to quantify how cable stiffness and tension govern the overall robot stiffness. Additionally, tensile tests were performed on the commonly used multi-strand cable, revealing that its tensile stiffness changes significantly with varying tension, especially in the pre-tensioning stage. Conversely, cable tensile stiffness remains constant in the elastic stage. Simulation results demonstrate that, for CDSMs using multi-strand cables, robot stiffness initially increases sharply with rising cable tension. However, once the cable enters its elastic stage, the overall robot stiffness shows a slight decreasing trend with tension increasing. Experimental results corroborates these findings, confirming the effect of cable tension across different tensile stages.

Future work will leverage these mechanistic insights to develop precision variable-stiffness control strategies, enhancing the adaptability and performance of CDSMs in constrained environments including minimally invasive surgery and industrial maintenance.

References

[1] Y.-J. Kim, S. Cheng, S. Kim, and K. Iagnemma, "A stiffness-adjustable hyperredundant manipulator using a variable neutral-line mechanism for minimally invasive surgery," *IEEE transactions on robotics*, vol. 30, no. 2, pp. 382–395, 2013.

[2] D. Wu, J. Li, D. Song, Z. Zhang, K. Wang, and C. Shi, "Development of a novel ball-and-socket flexible manipulator for minimally invasive flexible surgery," *IEEE Transactions on Medical Robotics and Bionics*, vol. 5, no. 2, pp. 278–288, 2023.

[3] X. Dong, D. Axinte, D. Palmer, S. Cobos, M. Raffles, A. Rabani, and J. Kell, "Development of a slender continuum robotic system for on-wing inspection/repair of gas turbine engines," *Robotics and computer-integrated manufacturing*, vol. 44, pp. 218–229, 2017.

[4] W. Ba, J.-C. Chang, J. Liu, X. Wang, X. Dong, and D. Axinte, "An analytical differential kinematics-based method for controlling tendon-driven continuum robots," *Robotics and Autonomous Systems*, vol. 171, p. 104562, 2024.

[5] B. Lin, W. Xu, W. Li, H. Yuan, and B. Liang, "Ex situ sensing method for the end-effector's six-dimensional force and link's contact force of cable-driven redundant manipulators," *IEEE Transactions on Industrial Informatics*, 2024.

[6] Y. Fang, X. Dong, A. Mohammad, and D. Axinte, "Design and control of a multiple-section continuum robot with a hybrid sensing system," *IEEE/ASME Transactions on Mechatronics*, vol. 28, no. 3, pp. 1522–1533, 2023.

[7] S. Liu, Z. Yang, Z. Zhu, L. Han, X. Zhu, and K. Xu, "Development of a dexterous continuum manipulator for exploration and inspection in confined spaces," *Industrial Robot: An International Journal*, vol. 43, no. 3, pp. 284–295, 2016.

[8] C. Yang, S. Geng, I. Walker, D. T. Branson, J. Liu, J. S. Dai, and R. Kang, "Geometric constraint-based modeling and analysis of a novel continuum robot with shape memory alloy initiated variable stiffness," *The International Journal of Robotics Research*, vol. 39, no. 14, pp. 1620–1634, 2020.

[9] P. Wang, S. Guo, X. Wang, and Y. Wu, "Design and analysis of a novel variable stiffness continuum robot with built-in winding-styled ropes," *IEEE Robotics and Automation Letters*, vol. 7, no. 3, pp. 6375–6382, 2022.

[10] S. Yeo, G. Yang, and W. Lim, "Design and analysis of cable-driven manipulators with variable stiffness," *Mechanism and Machine Theory*, vol. 69, pp. 230–244, 2013.

[11] A. Sobue, S. Komada, K. Yubai, and D. Yashiro, "Analysis of force/stiffness control of variable stiffness tendon driven arms," in *2018 12th France-Japan and 10th Europe-Asia Congress on Mechatronics*. IEEE, 2018, pp. 225–229.

[12] Y. Wang, G. Yang, K. Yang, and T. Zheng, "The kinematic analysis and stiffness optimization for an 8-dof cable-driven manipulator," in *2017 IEEE International Conference on Cybernetics and Intelligent Systems (CIS) and IEEE Conference on Robotics, Automation and Mechatronics (RAM)*. IEEE, 2017, pp. 682–687.

[13] S. Wolf and G. Hirzinger, "A new variable stiffness design: Matching requirements of the next robot generation," in *2008 IEEE International Conference on Robotics and Automation*. IEEE, 2008, pp. 1741–1746.

[14] J. Wang, G. Yang, K. Yang, and C.-Y. Chen, "Design of a flexure-based variable stiffness device for cable-driven joint modules," in *2015 IEEE International Conference on Robotics and Biomimetics (ROBIO)*. IEEE, 2015, pp. 2353–2358.

[15] C. A. Nelson, "On improving stiffness of cable robots," in *Cable-Driven Parallel Robots: Proceedings of the Third International Conference on Cable-Driven Parallel Robots*. Springer, 2018, pp. 331–339.

[16] T. Liu, Z. Mu, H. Wang, W. Xu, and Y. Li, "A cable-driven redundant spatial manipulator with improved stiffness and load capacity," in *2018 IEEE/RSJ International Conference on Intelligent Robots and Systems (IROS)*. IEEE, 2018, pp. 6628–6633.

[17] A. Alamdari, R. Haghighi, and V. Krovi, "Stiffness modulation in an elastic articulated-cable leg-orthosis emulator: Theory and experiment," *IEEE Transactions on Robotics*, vol. 34, no. 5, pp. 1266–1279, 2018.

[18] L. Zhang, Y. Gao, Z. Mu, L. Yan, Z. Li, and M. Gao, "A variable-stiffness planning method considering both the overall configuration and cable tension for hyper-redundant manipulators," *IEEE/ASME Transactions on Mechatronics*, 2023.

[19] Y. Yang, W. Chen, X. Wu, and Q. Chen, "Stiffness analysis of 3-dof spherical joint based on cable-driven humanoid arm," in *2010 5th IEEE Conference on Industrial Electronics and Applications*. IEEE, 2010, pp. 99–103.